Characterization of modified methylaluminoxane by ion mobility spectrometry mass spectrometry and ultra-high resolution Fourier-transform ion cyclotron resonance mass spectrometry

Ahmad Naim, Marie Hubert-Roux, Virginie Cirriez, Alexandre Welle, Aurelien Vantomme, Evgueni Kirillov, Jean-François Carpentier, Pierre Giusti, Carlos Afonso

Characterization of Modified Methylaluminoxane by Ion Mobility Spectrometry Mass Spectrometry and Ultra-High Resolution Fourier-Transform Ion Cyclotron Resonance Mass Spectrometry

Received 00th January 20xx,
Accepted 00th January 20xx

DOI: 10.1039/x0xx00000x

Ahmad Naim,[b,c‡] Marie Hubert-Roux,[b,c] Virginie Cirriez,[d] Alexandre Welle,[d] Aurelien Vantomme,[d] Evgueni Kirillov,[e] Jean-François Carpentier,[e] Pierre Giusti,*[a,c] and Carlos Afonso,*[b,c]

The analysis of methylaluminoxanes (MAOs) is strictly hampered by their high reactivity, in particular, toward oxygen and water. Commercially available modified MAO (MMAO) has revealed major interest as cocatalyst in olefin polymerization. The cocatalytic activity of MMAO is mainly linked to its chemical composition, which still lacks complete understanding about the precise structure of these complex molecules. To this aim, we have used in this study our recently developed piASAP technique to analyze air-sensitive MMAO-12 by mass spectrometry. The analysis of MMAO-12 was performed by ion mobility - mass spectrometry and Fourier transform mass spectrometry. The molecular analysis unveiled ten main family of MMAO clusters, which isotopic patterns are separated by *m/z* 57.999 corresponding to the MAO repeat unit (CH_3AlO). The collision cross section (CCS) values of these MMAO clusters were determined by ion mobility spectrometry (IMS). It was found that the detected lower molecular weight (MW) oligomers are probably representative segments of MMAO-12 that could be derived from a pyrolysis and hydrolysis, as it has been typically observed in the pyrolysis of polymers by Atmospheric Solid Analysis Probe (ASAP).

Introduction

Since the discovery of methylaluminoxane (MAO) by Kaminsky *et al.*,[1] MAO has become one of the most crucial activator for single-site olefin polymerization catalysts.[2] Its critical role in activating precatalysts by alkylation and ionization, forming highly active metal catalyst ion-pairs, has been well established.[3–5] In addition to activating precatalysts, MAO acts as a scavenger for impurities like moisture, oxygenates (*e.g.* O_2), Lewis bases, and Bronsted acids (*e.g.* acetylenes), which are reactive and often harmful toward the metal catalysts during polymerization process.[6] Despite of hundreds of publications in the last three decades on studying the role of MAO in olefin polymerization,[7] the structure and exact composition of this product, however, remains unclear; this is notably associated to the dynamic character of MAO.[3] In this regard, to get a better understanding of the action of MAO, activation efficiency and nature of the activated species,[8] it remains of paramount importance to characterize which clusters are present: degree of aggregation, functionalities.[9] MAO is produced from partial hydrolysis of trimethylaluminum (TMA), providing so-called "conventional" or "hydrolytic MAO" with variable residual amounts of TMA. Although, improved commercial processes with much higher yields have been developed,[10] the latter process has been modified by some manufacturers to afford higher yields of modified methylaluminoxanes (MMAOs) of increased solubility and stability.[11,12] There are different types of MMAOs that are formed from non-hydrolytic reactions, where-in some of the methyl groups are substituted by alkyl groups (common modifiers used are isobutyl and *n*-octyl groups), and each with different composition and properties.[13–15] Moreover, other types of MAOs produced by non-hydrolytic methods have also been reported.[15,16] MAO is a dynamic compound which rearranges rather fast upon time and also from stimuli received during analyses. Attempts at characterizing MAO by different spectroscopic techniques have been reported : infrared (IR),[17,18] ^{1}H and ^{13}C NMR,[19–22] ^{27}Al NMR[23–27] (including solid-state ^{27}Al NMR[28,29]), diffusion spectroscopy (DOSY),[30–32] and EPR.[33,34] These experimental studies have also been coupled with theoretical modeling approaches,[35–42] eventually providing some information on MAO's nature and proposition of possible structures. However, conclusions often varied amongst research groups,[41]and one still lacks complete understanding about the precise structure of these complex, dynamic molecules.[14]

Advanced mass spectrometric methods have been employed in this course to determine the composition and structure of

[a] TotalEnergies Research and Technologies Gonfreville BP 27, 76700 Harfleur, France.
[b] Univ Rouen Normandie, INSA Rouen Normandie, CNRS, Normandie Univ, COBRA UMR 6014, INC3M FR 3038, F-76000 Rouen, France.
[c] TotalEnergies RC - CNRS Joint Laboratory C2MC: Complex Matrices Molecular Characterization, University of Pau, University of Rouen, CNRS, 64053 Pau, France.
[d] TotalEnergies Research and Technologies Feluy, Zone Industrielle C B-7181 Feluy, Belgium.
[e] Univ Rennes, CNRS, ISCR (Institut des Sciences Chimiques de Rennes) UMR 6226, 35000 Rennes, France.

† Electronic Supplementary Information (ESI) available: [details of any supplementary information available should be included here]. See DOI: 10.1039/x0xx00000x

MAO, especially in the last decade. It has been found that hard ionization methods were not suitable to furnish a consistent information.[36] However, electrospray ionization (ESI), a softer ionization method, has proved its capability to produce gas phase MAO ions using additives in a polar solvent. The first investigation of MAO in tetrahydrofuran (THF) by electrospray ionization mass spectrometry (ESI-MS) has afforded a positive ion spectrum displaying mainly oxidized MAO species (*i.e.*, $[OAlOMe]_n$);[43] this is probably due to the lack of anaerobic ESI conditions.[44] Likewise, McIndoe *et al.* have studied the composition,[45] aging,[46] oxidation,[47] and real-time formation of hydrolytic MAO[48] by ESI-MS. The formation of a major MAO ion at *m/z* 1853 was achieved after combining MAO with Cp_2ZrMe_2, octamethyltrisiloxane (OMTS), or $Bu_4N^+Cl^-$ in fluorobenzene. This anion has been proposed to be $[(MeAlO)_{23}(Me_3Al)_7Me]^-$.[45] The composition of the observed MAO anions in ESI-MS analysis was compatible with the range of the average composition of MAO $[Me_{1.4\text{-}1.5}AlO_{0.75\text{-}0.8}]$ determined independently by solution ^{1}H NMR spectrocopy.[19] Also, McIndoe *et al.* have studied the effect of aging on the composition of MAO by ESI-MS; these studies revealed a slow, systematic conversion of low molecular weight (MW) MAO oligomers to higher MW species through addition of (MeAlO) and TMA units over time and this has been proposed as a marker for MAO aging.[46] In a recent study by the same group, monitoring of MAO oxidation by ESI-MS revealed that exposing MAO to oxygen (O_2) results in the formation of oxidized MAO oligomer anions with the general formula $[(MeAlO)_x(Me_3Al)_y(Me_2AlOMe)_zMe]^-$, where one molecule of Me_3Al is liberated from an unoxidized MAO oligomer and replaced by a Me_2AlOMe group. This was confirmed by the loss of a unit of 88 Da from the oxidized MAO anion in MS/MS studies at high collision energy. Also, ^{1}H NMR spectroscopy indicated the presence of resonances between $^\delta$H 4.0 and 4.6 ppm assigned to OMe groups.[47] A very recent real-time analysis study of the formation of MAO by McIndoe *et al.* has shown that hydrolysis of TMA involves a short-lived formation of MAO anions of various compositions $[(MeAlO)_x(Me_3Al)_yMe]^-$ (where x = 7-9; y = 4) that are probably derived from MAO oligomers generated in the early stages (in the second scale) from a cascade of hydrolysis, oligomerization, and isomerization reactions to form higher MW MAO anions.[48] MMAOs have shown co-catalyst activity that is equivalent to, or even higher than, that of polymethylaluminoxane (MAO), and recently their application as cocatalyst has attracted much attention.[49–53,16] The negative ion mode analysis of non-hydrolytic MAO (MMAO-12) using 5 mol% OMTS by electrospray ionization mass spectrometry (ESI-MS) revealed a wide range of ions (*m/z* 800 to 3000). The predicted ions related to MAO/MMAO and oxidized species appeared at extremely low intensities and their assignment was based on nominal mass, precluding their confirmation by MS/MS analyses.[54] It was also noted that the anionic distribution of non-hydrolytic MAO (MMAO-12) was completely different from that of hydrolytic MAO (obtained by hydrolysis of $AlMe_3$) analyzed under the same conditions using OMTS as donor additive.[55] The aim of this attempt was to obtain direct insight into the composition of MMAO without pre-treatment by additives, which could limit the detection of a large class of MMAO ions due to the difference in reactivity of neutral methylaluminoxane towards the additive. This direct analysis was undertaken to ultimately improve their activating efficiency in olefin polymerization.

In this study, we first report on the analysis of MMAO-12 by Paraffin Inert Atmospheric Solids Analysis Probe (piASAP) on a travelling wave ion mobility time of flight instrument (TWIMS-TOF) and Fourier-transform ion cyclotron resonance (FTICR) mass spectrometer. To our knowledge, this is the first time MMAO is analyzed by such combined techniques. The analysis was performed using recently developed paraffin inert ASAP (piASAP) technique that has proven its efficiency in analysis of highly air sensitive metallocenes.[56]

EXPERIMENTAL SECTION

Materials. Modified methylaluminoxane (MMAO-12) (7 wt% Al in toluene) was purchased from Sigma-Aldrich and stored in the freezer upon receipt. The melting point tubes (Length: 100 mm, Ø ext.: 1.55 mm, Ø int.: 1.15 mm) used in all experiments were provided from VWR supplier. The white paraffin pellets (Sigma-Aldrich) used in the preparation experiments meet the analytical specifications of Ph. Eur. with m.p. in the range 43−95 °C.

Sample Preparation. In a typical piASAP experiment, the MMAO-12 sample was warmed to room temperature (no precipitations were observed) and transferred to the glovebox (GP Campus, Jacomex; < 2 ppm O_2, < 2 ppm H_2O). In the glovebox, a 1 mL plastic syringe with a needle was used to transfer the MMAO solution into a glass capillary sealed at one end. Then, the other end was closed by a paraffin plug. The sealed glass capillary was transported to the ASAP source. It is noteworthy to mention that the glass capillary was filled to 80 mm level in order to avoid any contact of the MMAO solution with the paraffin to ensure fully anaerobic conditions before analysis.

Instrumentation. Ion mobility spectrometry - mass spectrometry (IMS-MS) experiments were performed using a hybrid travelling wave ion mobility spectrometry - quadrupole - time-of-flight mass instrument (Synapt G2, Waters Corp. Wilmslow, UK) fitted with an atmospheric solid analysis probe (ASAP) source. This instrument incorporates a traveling wave (T-Wave)-based ion mobility spectrometry device (TWIMS). The instrument and the T-Wave device have been described in details elsewhere.[57,58] The ASAP mass spectra were recorded in positive ion mode with *m/z* 50-1200 range using W reflectron mode. The TWIMS-MS cell was operated with N_2 as a buffer gas. The following acquisition parameters were adopted for all experiments: Corona voltage 4.0 V, probe temperature 650 °C, source temperature 140 °C, drying gas flow 1200 L h^{-1}, helium cell gas flow 180 mL min^{-1}, ion mobility cell gas flow rate 80 mL min^{-1}, IMS wave height 40 V, IMS wave velocity 600 m s^{-1}, and IMS wave delay 1200 µs. The time-of-flight (TOF) mass spectrometer was externally *m/z* calibrated using a sodium formate solution before sample analysis. Data treatment was carried out with the MassLynx software, version 4.1, and DriftScope software, version 2.9 (Waters, Manchester, UK). For TWIMS calibration, DTCCS values in N_2 of dextran were used.[59]

For collision cross section (CCS) determination, TWIMS spectra were fitted to Gaussian curves with OriginPro 2016 to obtain experimental drift times with maximum accuracy. The collision cross section (CCS) of MMAO was calculated based on the method described by Smith *et al.* using a reduced collision cross section (Ω') (Equation 1, supporting information),[60] which depends on ion mobility of molecules (including the charge z and reduced mass μ). The method uses a correlation between this reduced collision cross section Ω' and the drift time using a power function (Equation 2, supporting information) where A is a correction factor for temperature and pressure and B as a compensation for the non-linear effect of the TWIMS system. In our case, this equation was linearized by using natural logarithms, in order to obtain a linear regression.

FTICR experiments were carried out with a Bruker Solarix XR (Bruker Daltonik GmbH, Bremen, Germany) instrument equipped with a 12 T actively shielded superconducting magnet and a dynamically harmonized ICR cell. Mass spectra were acquired with 8 M data points with a transient time of 3.35 s resulting in a resolution of about 10^6 at *m/z* 400 in the magnitude mode. Mass spectra were recorded between *m/z* 122 and 2000. The sample introduction was performed using direct insertion probe (DIP) atmospheric pressure chemical ionization (APCI) source. The source and acquisition parameters of DIP-APCI analysis were as follows: nebulizer gas temperature 300 °C or 350 °C, drying gas temperature 200 °C, drying gas flow 2 L min^{-1}, nebulizer gas pressure 2.3 bar, capillary voltage 2000 V, ion accumulation time 0.020 s and corona needle current 3000 nA. The data was processed using Data Analysis v5.0 software (Bruker Daltonik GmbH, Bremen, Germany) and it was internally calibrated using list of paraffin ions. It is noteworthy to mention that both ASAP and DIP-APCI sources present same ionization processes and we will refer only to ASAP in the manuscript.

Results and discussion

In the glovebox, capillary tubes were filled by freshly ordered MMAO-12 (7 wt % Aluminum in toluene) and then sealed with paraffin for analysis. The capillary tube was then introduced into the ASAP ionization sources coupled to a TWIMS-Q-TOF or a FTICR instrument. Being a mixture of alkanes, paraffin does not ionize well in comparison to polar analytes under ASAP conditions, but melts quickly, releasing the MMAO-12 solution in the source. Then, the sample is desorbed by a hot nitrogen flow and ionized by a nitrogen plasma generated by corona discharge.[61] In previous studies, coupling of ion mobility to mass spectrometry has allowed a new dimensional separation for analysis of complex mixtures.[62,63] Ion mobility spectrometry - mass spectrometry (IMS-MS) has become an attractive analytical technique in chemical and biological research areas.[64,65] Separation in this technique is usually based on *m/z*, size and shape of the analyzed molecules in which smaller size ions assume shorter drift times (ms) in comparison to larger size ions that exhibit longer drift times. This is due to the fact that small ions are transferred inside the drift tube faster than bulkier ions (i.e. small ions are less interacting with the drift gas that can be He or N_2). With the TWIMS-Q-TOF, a bidimensional separation is achieved, adding to the *m/z* a separation based on drift time that is related on the ions size and shape.

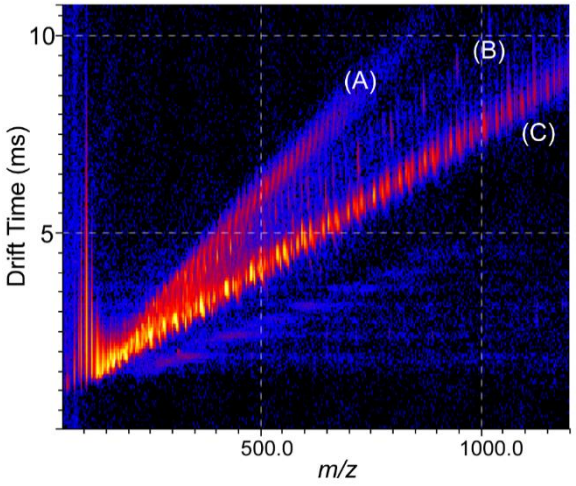

Figure 1. 2-Dimensional plot of drift time as a function of m/z of MMAO-12 measured at cone voltage of 20 V recorded in a TWIMS-Q-TOF instrument.

The 2-D plot of drift time as a function of *m/z* of MMAO-12 (Figure 1) shows the presence of three series of ions (A, B, and C). It is known that, for singly charged species, ions of the same family tend to follow straight line in drift time vs *m/z* plots.[65] The mass spectra of the three series of ions (A, B, and C) were extracted from the drift time vs *m/z* plot (Figure 2). The first series (A) consists of paraffin ions with higher drift times, and the second series (B) that is spanning the middle area between series A and C represents ions that are corresponding to residual TMA. The third series (C) is comprised of MMAO-12 ions with lower drift times and that are resolved according to their size and shape. Hence, the paraffin, TMA and MMAO-12 ions can be easily evidenced from the 2D map. This is consistent with previous works showing particularly high drift time to the non-polar and elongated paraffin molecules whereas more polar molecules tend to form more compact ions and lower drift times.[66–68] The bulk mass spectrum (*i.e.* without extraction) of MMAO-12 (Figure S1) revealed the high complexity of MMAO-12; isotopic patterns of MMAO-12 ions are mixed with other patterns related to TMA and paraffin (low intensity signals) along the whole *m/z* range (50–980). Noteworthy, it was highly difficult to assign unambiguously the molecular formulae (*i.e.* many possible formulas considering C, O, H and Al elements) for the observed ions of MMAO-12 in our high resolution TOF-MS data. Obviously, higher mass resolution and mass accuracy was needed (Figure S2 to S3). For this purpose, we have analyzed MMAO-12 by piASAP on an ultra-high-resolution FTICR-MS to determine the composition of this complex mixture. In previous studies, FTICR-MS has been used to analyze and differentiate various complex organic mixtures such as crude oil.[69] Since MMAO exhibits also a highly complex nature and composition, we have analyzed a freshly ordered MMAO-12 solution (7 wt% aluminum in toluene) by ASAP without diluting the commercial solution.[56]

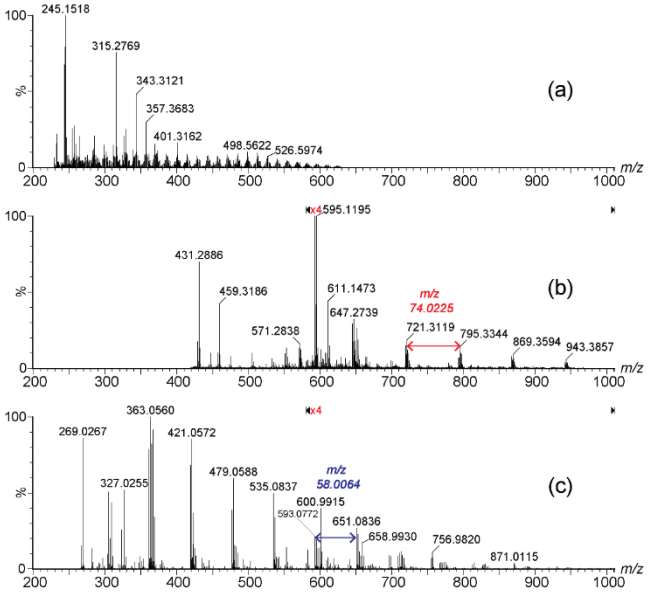

Figure 2. Mass spectra of piASAP analysis of MMAO-12 extracted from the IMS-MS data showing (a) paraffin ions (Series A), (b) TMA ions (Series B), and (c) MMAO-12 (series C).

The piASAP mass spectrum of MMAO (Figure 3) recorded in positive mode was very similar to that obtained by TWIMS-Q-TOF. It reveals the presence of ten main different MMAO family groups (*i.e.* most intense ion series) comprised of signals that are separated by *m/z* 57.999, *i.e.* the MAO repeat unit (CH_3AlO) (vide-infra). These observed signals of different family groups of MMAO belong to various aluminum species (Al_{3-14}) that range between *m/z* 193.017 and 832.995 (Figure S4); and, each Al class of MMAO cluster belong to different oxygen classes that can range between O_4 and O_{17} classes. For instance, Al_8 clusters in the mass range *m/z* 535–547 encompass different number of oxygen atoms (O_7, O_8, O_9, O_{10}, O_{11}, O_{12} and O_{13}) of different relative intensities (Figure 3). The difference in mass between adjacent O classes or alternate Al_xO_y (where x = 8; y = 7, 8, 9, 10, 11, 12, 13) core structures (i.e. Al_8O_7 to Al_8O_8 with *m/z* 535.07967 and 537.058880, respectively) is equal to *m/z* 1.979 that corresponds formally to removal of a CH_2 group and addition of one oxygen atom. The difference in mass is related to different MMAO family structures. This is likely due to hydrolysis, in which one or more methyl $-CH_3$ is replaced by –OH group(s) of MMAO structure after reaction with water, eventually eliminating methane. Due to the high reactivity of MMAO-12, this partial adventitious hydrolysis may arise during the ionization step. Since ASAP ionization is more energetic than ESI, possibly many MMAO ions (*i.e.* ESI silent MMAO), which could not be ionized by ESI, could be detected by ASAP that does not require polar solvents or soluble molecules.[44] This shows the importance to analyze this complex mixture by versatile MS techniques in order to access vast information about its diverse composition. The comparison of relative intensities of aluminum classes of MMAO-12 (Figure S5) demonstrates that Al_8 and Al_9 classes are the most abundant ones, while (Al_7, Al_{10}) and (Al_6, A_{11}, Al_{12}, Al_{13}, Al_{14}) aluminum groups display very close relative intensities; all other Al classes are present at very low abundance. Comparison of the relative intensities of oxygen classes of MMAO suggests that oxygen groups (O_9, O_{10}, O_{11}, O_{12}), (O_7, O_8, O_{13}), (O_{14}, O_{15}), (O_{16}, O_{17}) and (O_1, O_2, O_3, O_4, O_5, O_6) have a comparable or very close relative abundance (Figure S6). The molecular formula ions for all identified family groups of MMAO clusters are listed in Tables S1 to S5.

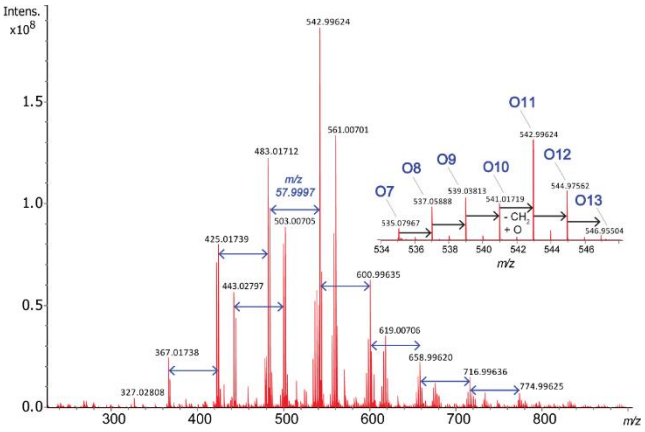

Figure 3. piASAP FTICR mass spectrum of MMAO-12 showing ions series separated by 57.9997 u (CH_3AlO). The zoomed areas showcase distribution of Al_8O_y (*y*= 7, 8, 9, 10, 11, 12 and 13). MMAO-12 clusters in piASAP FTICR mass spectrum of MMAO-12 in mass range (*m/z* 534-547).

Modified Kendrick Plot of MMAO

One of the direct and convenient ways to represent the data from ultra high-resolution mass spectrometry is by using Kendrick plots.[70–72] This is a graphical representation of apparent Kendrick mass defect (aKMD) as a function of apparent nominal mass (aNM) for ions observed in the mass spectrum. It has been applied to represent extremely large data sets in the analysis of highly complex mixtures of petroleum,[69,73] environmental samples,[74–77] metabolomics[78] and polymers.[79] KMD is the difference between Kendrick mass (KM) and nominal mass (*i.e.* the nearest integer mass, abbreviated as NM). The reference that was used in this plot is the repeat MAO unit CH_3AlO of MMAO. The KM value was calculated by multiplication of IUPAC mass (*m/z* calculated for each ion) by 58.00000 (*i.e.* the nominal mass of CH_3AlO) and then dividing by 57.999928 (*i.e.* the exact mass of CH_3AlO):

KMD = Kendrick mass (KM) – nominal mass (NM)

KM = IUPAC mass × (58/57.999928)

In this case, species that differ only by their number of CH_3AlO units will present the same KMD value and will be observed as horizontal lines in the KMD *vs.* NM plot. The modified Kendrick plot of MMAO-12 determined in the present study is shown in Figure 4. It is obvious that MMAO clusters are separated into homologous series (bubbles in navy color) that have the same chemical core, but different number of CH_3AlO units. Consequently, different family groups of MMAO clusters can be recognized according to their different Kendrick mass defect (KMD) while MMAO clusters of the same family groups have common KMD (*i.e.* aligned horizontally in the graph). So,

the MMAO clusters of different family groups can now be readily identified because the KMD of MMAO ions in a given group is displaced vertically from those of other groups. In the present modified Kendrick plot for MMAO-12, ten family groups of MMAO clusters were identified and the relative intensity of MMAO ions was adopted to be greater or equal to 0.2% (Figure S7). For each identified main MMAO-12 family groups (1, 3, 5, 7 and 9) are found their hydrated (H_2O) analogue groups (2, 4, 6, 8 and 10), respectively.

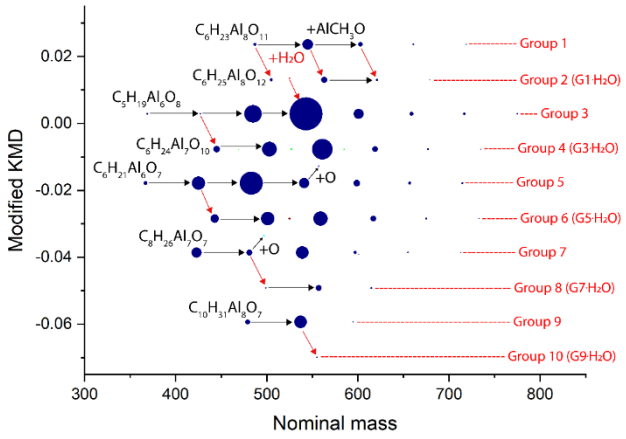

Figure 4. Plot of modified Kendrick mass defect (KMD) *vs.* nominal Kendrick mass (NM) for MMAO ions of nominal mass from 300 to 800 Da in the piASAP FTICR mass spectrum of MMAO-12. N.B. The relative intensity of the ions was filtered to be greater or equal to 0.2 %.The size of the bubbles is proportional to the ion intensity.

Those hydrated analogues are probably formed in the MS instrument due to the unavoidable presence of minute amounts of water, possibility from N_2 gas[80] or instrumental surfaces; these hydrated analogues are probably very short lived, since subsequent hydrolysis of Al–Me groups is anticipated within seconds, minutes, hours, at most. The MMAO ion in red color corresponds to $C_8H_{26}Al_9O_{10}$ (–0.1 ppm) molecular formula found at *m/z* 524.985972 Da. The sequence of MMAO ions in green color at *m/z* 469.007338, 527.007222, 585.007197 was attributed to $C_8H_{24}Al_7O_{10}$ (–0.4 ppm), $C_9H_{27}Al_8O_{11}$ (–0.2 ppm) and $C_{10}H_{30}Al_9O_{12}$ (–0.3 ppm), respectively. The MMAO ions in blue, wine, cyan, magenta colors are referred to $C_9H_{30}Al_9O_{11}$ (*m/z* 557.012114, error 0.0 ppm), $C_{10}H_{29}Al_8O_{10}$ (*m/z* 525.027684, error 0.3 ppm), $C_9H_{29}Al_8O_9$ (*m/z* 497.032929, error 0.0 ppm), $C_{11}H_{34}Al_9O_{12}$ (*m/z* 601.038582, error –0.4 ppm), subsequently. The MMAO ions in blue and cyan colors are probably formed from oxidation (*i.e.* insertion of oxygen atom) of MMAO ions found in Groups 5 and 7, respectively. The proposed structures of identified MMAO groups are shown in Scheme 1. The difference between the main MMAO groups (Groups 1, 3, 5, 7 and 9) is related to the partial hydrolysis degree of the MMAO structure, in which 4 methyl (Group 1), 3 methyl (Group 3), 2 methyl (Group 5) and 1 methyl (Group 7) groups are replaced by hydroxy groups to the structure (with concomitant release of methane molecule(s)). The number of repeat units (n) of (CH_3AlO) is ranging between 1 and 12. However, the only detected MMAO ions of Group 9 and 10 are referred to non-hydrolyzed MMAO structures, where n is ranging between 5 and 10. It is noteworthy to mention that no *n*-octyl groups was detected among the main identified MMAO groups. This observation is common as MAO-based ions are sensitive to hydrolysis despite extensive precautions such as purging the source compartment with inert gas and safe handling of the sample under anaerobic conditions prior to analysis.[81] One might expect higher MW ions for non-hydrolytic MMAO-12,[82] but we have probably a pyrolysis that forms smaller oligomers (at lower MW) that are representative of primary MMAO-12 ions (*e.g.* non-hydrolyzed oligomers of group 9 and 10), as it has typically been observed in the pyrolysis of polymers.[67] The non-observed "modified" part of MMAO-12 (in this case *n*-octyl) was also probably pyrolyzed with primary large MMAO clusters. For further information, the molecular formula ions for all identified family groups (in navy color) of MMAO clusters are listed in Tables S1-S5.

CCS of MMAO clusters

As mentioned above, the exact structure of MAO clusters has remained uncertain[47,48] although many efforts have been made, in particular by performing theoretical DFT studies.[83] After determining unambiguously molecular formulas of MMAO ions, we assessed the 3D structure of the detected MMAO-12 oligomers using ion mobility spectrometry - mass spectrometry.

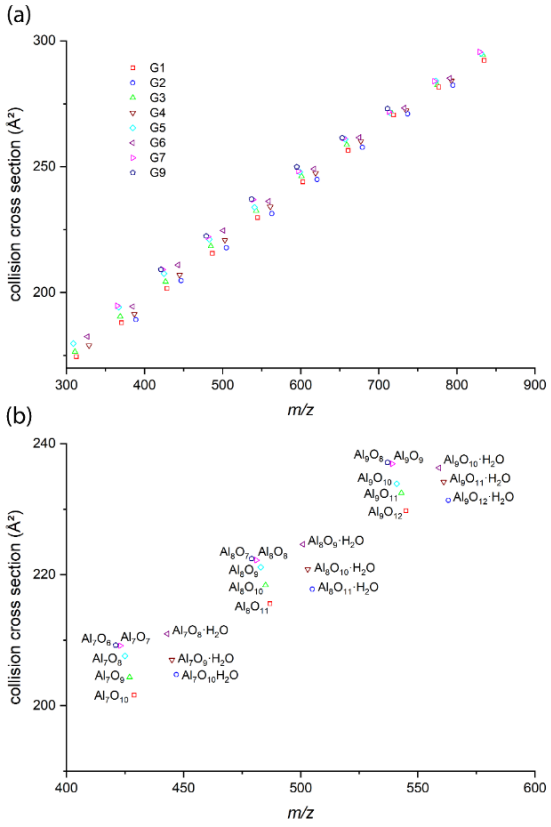

Figure 5. (a) Graphical representation of collision cross section (CCS) against *m/z* for MMAO clusters in Groups 1-9 observed in modified Kendrick plot between *m/z* 300-900. (b) Distribution of MMAO clusters of different CCS (Å²) in Groups 1, 2, 3, 4, 5, 6, 7 and 9 between *m/z* 400-600.

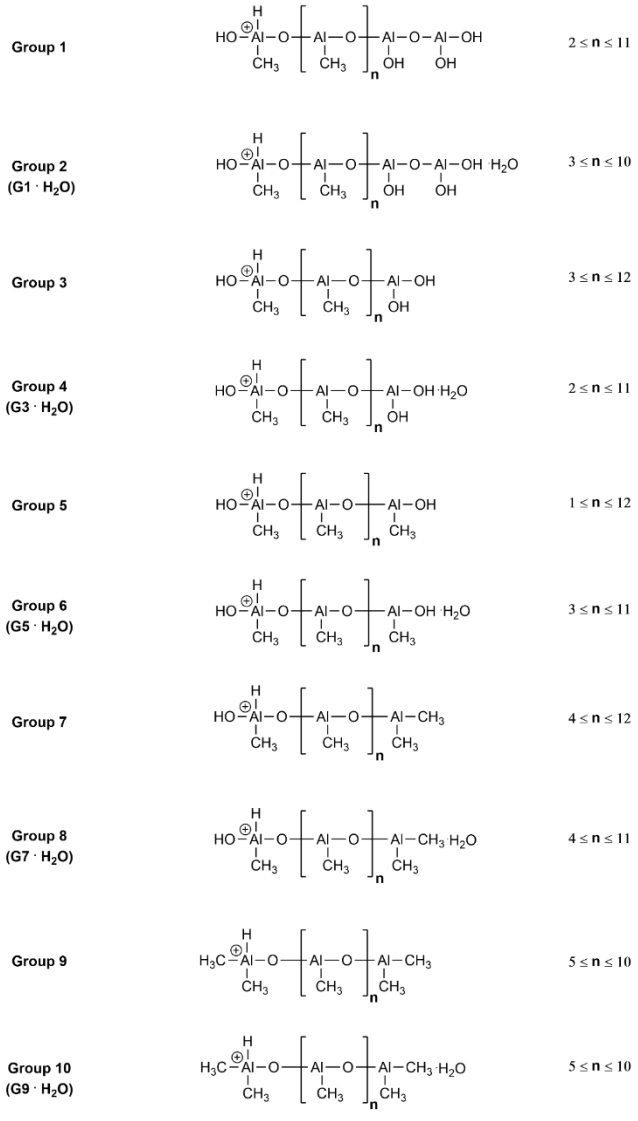

Scheme 1. Proposed detected MMAO structures of Groups 1–10.

To this end, we have determined the collision cross section (CCS in Å²) of MMAO clusters in Groups 1–10 that were observed in the modified Kendrick plot (Figure 4). In this course, the CCS of MMAO-12 ions was estimated using calibration with compounds of known CCS values.[59] The correlation obtained from standards of dextran with known CCS and their drift time, measured using the TWIMS cell, were used to estimate the CCS of MMAO clusters. The CCS of MMAO family Groups 1–10 are presented in Figure 5a, and the CCS numerical values are shown in Table S1-5. The CCS of MMAO oligomers ranges between 146 and 296 Å², and this is related to the *m/z*, size, and shape of the clusters. The MMAO ions of Group 9 (*i.e.* non-hydrolyzed MMAO structures) are comprised mostly of clusters with lower number of oxygen atoms between *m/z* 400–750 (see Figure 5a). These ions are aligned linearly (pentagon shape, navy color, Figure 5a) that has a higher slope (*i.e.* higher CCS values) than other partially hydrolyzed MMAO oligomers. On the other hand, MMAO ions that feature significant differences of CCS values are distributed in Groups 1-9 between *m/z* 400–600 (Figure 5b). The variation of CCS value significantly depends on the number of oxygen atoms in each MMAO cluster of the same aluminum class (*i.e.* same number of aluminum atoms). For instance, MMAO clusters with 8 aluminum atoms (Al_8) in the range *m/z* 475–510 showed CCS values in decreasing order with the increase of the number of oxygen atoms: CCS(Al_8O_7, Group 9) ≈ CCS (Al_8O_8, Group 7) > CCS (Al_8O_9, Group 5) > CCS (Al_8O_{10}, Group 3) > CCS (Al_8O_{11}, Group 1). The latter $C_7H_{26}Al_9O_{12}$ (*m/z* 544.975, Group 1) and $C_7H_{28}Al_9O_{13}$ (*m/z* 562.986, Group 2) clusters had very small difference in CCS values (Δ = 1.6 Å²), which is related to the addition of H_2O molecule (*i.e.* hydration). These results suggest that addition of oxygen atoms to MMAO clusters leads to the formation of more compact MMAO structures (*i.e.* lower CCS values) that are intra-molecularly interacting with the replacement of methyl by polar hydroxyl groups (see Scheme 1).

In the same way, the CCS of repeat motif ($AlCH_3O$) of MMAO between subsequent ions of the same family group can vary significantly by addition of a repeat unit as shown in Table 1. For example, the CCS of $AlCH_3O$ group in MMAO family Group 1

Table 1. Variation of CCS of CH_3AlO within the same and different MMAO family groups.

Group	General formula ($[M+H]^+$)	CCS range of MMAO ions (Å²)	CCS range of $AlCH_3O$ group (Å²)	Average CCS of $AlCH_3O$ group (Å²)
1	$(CH_3)(OH)_4(H)Al_3O_2$ + n ($AlCH_3O$) (2≤n≤11)	174.6 to 292.1	10.6 to 14.2	13.1 ± 1.4
2	$(CH_3)(OH)_4(H)Al_3O_2$ + n ($AlCH_3O$)·H_2O (3≤n≤10)	189.3 to 282.3	11.4 to 15.5	13.3 ± 1.2
3	$(CH_3)(OH)_3(H)Al_2O$ + n ($AlCH_3O$) (3≤n≤12)	176.5 to 294.4	11.4 to 14.1	13.1± 1.0
4	$(CH_3)(OH)_3(H)Al_2O$ + n ($AlCH_3O$)·H_2O (2≤n≤11)	179.1 to 284.1	11.8 to 15.5	13.1 ± 1.2
5	$(CH_3)_2(OH)_2(H)Al_2O$ + n ($AlCH_3O$) (1≤n≤12)	146.4 to 295.0	10.4 to 18.9	13.5 ± 2.2
6	$(CH_3)_2(OH)_2(H)Al_2O$ + n ($AlCH_3O$)·H_2O (3≤n≤11)	182.5 to 285.1	11.7 to 16.5	12.8 ± 1.6
7	$(CH_3)_3(OH)(H)Al_2O$ + n ($AlCH_3O$) (4≤n≤12)	194.8 to 295.6	10.5 to 14.7	12.6 ± 1.5
8	$(CH_3)_3(OH)(H)Al_2O$ + n ($AlCH_3O$)·H_2O (4≤n≤11)	--	--	--
9	$(CH_3)_4(H)Al_2O$ + n ($AlCH_3O$) (5≤n≤10)	209.2 to 273.1	11.5 to 14.7	12.8 ± 1.3
10	$(CH_3)_4(H)Al_2O$ + n ($AlCH_3O$)·H_2O (5≤n≤10)	--	--	--

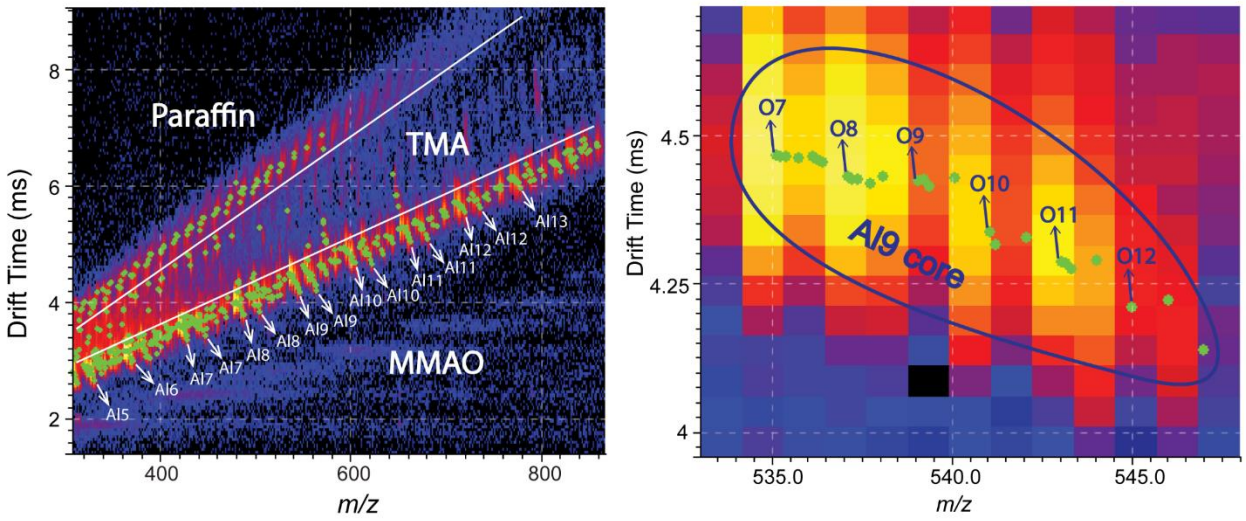

Figure 6. (a) left side, 2-dimensional plot of drift time as a function of *m/z* of MMAO-12: distribution of Al classes of MMAO clusters along *m/z* 300-850. (b) Right side, 2-Dimensional plot of drift time as a function of *m/z* of MMAO-12: distribution of O classes of MMAO Al9 core cluster at *m/z* 533-548.

varied from 10.6 to 14.2 Å². We presume that this variation is due to the different placement or localization of CH_3AlO groups within the 3D structure of MMAO oligomers. Also, MMAO family Groups 2–9 showed a similar variation of CCS of $AlCH_3O$ group between consecutive MMAO clusters of the same group. In parallel, the bidimensional plot of drift time as a function of *m/z* clearly showed that, as the number of Al atoms within the MMAO clusters increases, the drift time increases (Figure 6a). This latter increase is usually associated with the increase of the size and the CCS value ($Al_3 < Al_4 < Al_5 < Al_6 < Al_7 < Al_8 < Al_9 < Al_{10} < Al_{11} < Al_{12} < Al_{13} < Al_{14}$) due to the addition of CH_3AlO groups (Figure 5). However, as discussed before, in the same Al clusters class (Figure 6b), one can notice that the drift time decreases as the oxygen number within the MMAO oligomers increases. This decrease in the drift time is accompanied with the loss of a methyl group and incorporation of a hydroxyl group. The latter incorporation of O atoms leads to the formation of more compact MMAO oligomer structures (*e.g.* the Al_9O_{12} cluster is more compact than Al_9O_7) (Figure 6b) and this is compatible with the calculated CCS values (Tables S1–S5). This phenomenon is probably accompanied with structural rearrangements in the partially hydrolyzed MMAO oligomers and is consistent with our previous results.[68]

Conclusions

We have presented the first analytic results of commercially-available modified MAO (MMAO-12) by atmospheric solid analysis probe (ASAP) using the recently developed piASAP technique. The analysis of MMAO-12 by piASAP TWIMS-TOF shows in the drift time vs *m/z* 2D plot three ion series corresponding to paraffin, free TMA, and the desired MMAO cluster ions. The resolution and mass accuracy of the TOF mass spectrometer was not sufficient to unambiguously assign the molecular compositions of the observed MMAO patterns, and it was indispensable to use ultra-high-resolution mass spectrometry (FTICR-MS). The piASAP-FTICR mass spectrum of MMAO-12 allowed confident determination of the molecular compositions of at least 10 MMAO family groups. The MMAO clusters in each family group are separated by *m/z* 57.999, *i.e.* the MAO repeat unit (CH_3AlO) as it is also shown in the modified Kendrick plot. Also, we established the collision cross section (CCS) values of the most abundant MMAO clusters by ion mobility spectrometry (IMS). We have noticed a probable pyrolysis that affords smaller oligomers (at lower MW) that are representative of primary MMAO-12 molecules, as it has typically been observed in the pyrolysis of polymers. We believe that our results will open the way to predict more precisely the structural diversity of the detected MMAO oligomers of MMAO-12 from the proposed structures, data of collision cross section of each MMAO oligomer (*i.e.* cluster) and theoretical DFT calculations to ultimately predict the 3D structures of primary MMAO molecules from these oligomers.

Author Contributions

AN has performed experiments, data treatment and manuscript writing, correcting and editing. MHR has assisted in experiments. MHR, CA, PG, JFC, EK VC, AW and AV have contributed to the discussion of data and editing of the manuscript.

Conflicts of interest

There are no conflicts to declare.

Acknowledgements

This work has been partially supported by the University of Rouen Normandy, INSA Rouen Normandy, the Centre National de la Recherche Scientifique (CNRS), European Regional Development Fund (ERDF), Labex SynOrg (ANR-11-LABX-0029), Carnot Institut I2C, the graduate school for research XI-Chem (ANR-18-EURE-0020 XL CHEM), the European Union's Horizon 2020 Research Infrastructures program (Grant Agreement

731077) and by Region Normandie. Access to a CNRS FTICR research infrastructure (FR2054) is gratefully acknowledged.

Notes and references

Corresponding Authors

*email: carlos.afonso@univ-rouen.fr
*email: pierre.giusti@totalenergies.com

Present Addresses

‡ AN : Université Paris-Saclay, CEA, INRAE, Département Médicaments et Technologies pour la Santé (MTS), MetaboHUB, Gif sur Yvette, France

1 A. Andresen, H.-G. Cordes, J. Herwig, W. Kaminsky, A. Merck, R. Mottweiler, J. Pein, H. Sinn and H.-J. Vollmer, *Angew. Chem. Int. Ed. Engl.*, 1976, **15**, 630–632.
2 W. Kaminsky, *Macromolecules*, 2012, **45**, 3289–3297.
3 E. Y.-X. Chen and T. J. Marks, *Chem. Rev.*, 2000, **100**, 1391–1434.
4 M. Bochmann, *J. Organomet. Chem.*, 2004, **689**, 3982–3998.
5 M. Bochmann, *Organometallics*, 2010, **29**, 4711–4740.
6 D. B. Malpass, in *Handbook of Transition Metal Polymerization Catalysts*, John Wiley & Sons, Ltd, 2010, pp. 1–28.
7 V. Busico, *Dalton Trans.*, 2009, 8794–8802.
8 X. Desert, J.-F. Carpentier and E. Kirillov, *Coord. Chem. Rev.*, 2019, **386**, 50–68.
9 E. Zurek and T. Ziegler, *Prog. Polym. Sci.*, 2004, **29**, 107–148.
10 U.S. Patent No. 5,663,394, 1997.
11 Japanese Patent Laid-Open Publications No. 2000119278, .
12 Japanese Patent Laid-Open Publications No. 2000119279, .
13 In *Introduction to Industrial Polyethylene*, John Wiley & Sons, Ltd, 2010, pp. 71–84.
14 EP 1352913A1, 2003.
15 U.S. Patent No. 5,381,109, 1998.
16 R. Tanaka, *Polym. J.*, 2020, **52**, 661–670.
17 E. Giannetti, G. M. Nicoletti and R. Mazzocchi, *J. Polym. Sci. Polym. Chem. Ed.*, 1985, **23**, 2117–2134.
18 M. Ystenes, J. L. Eilertsen, J. Liu, M. Ott, E. Rytter and J. A. Støvneng, *J. Polym. Sci. A Polym. Chem.*, 2000, **38**, 3106–3127.
19 D. W. Imhoff, L. S. Simeral, S. A. Sangokoya and J. H. Peel, *Organometallics*, 1998, **17**, 1941–1945.
20 L. Cocco and D. P. Eyman, *J. Organomet. Chem.*, 1979, **179**, 1–6.
21 L. Resconi, S. Bossi and L. Abis, *Macromolecules*, 1990, **23**, 4489–4491.
22 D. Cam and U. Giannini, *Makromol. Chem.*, 1992, **193**, 1049–1055.
23 R. Benn, A. Rufińska, H. Lehmkuhl, E. Janssen and C. Krüger, *Angew. Chem. Int. Ed. Engl.*, 1983, **22**, 779–780.
24 L. A. Nekhaeva, G. N. Bondarenko, S. V. Rykov, A. I. Nekhaev, B. A. Krentsel, V. P. Mar'in, L. I. Vyshinskaya, I. M. Khrapova, A. V. Polonskii and N. N. Korneev, *J. Organomet. Chem.*, 1991, **406**, 139–146.
25 T. Sugano, K. Matsubara, T. Fujita and T. Takahashi, *J. Mol. Catal.*, 1993, **82**, 93–101.
26 M. R. Mason, J. M. Smith, S. G. Bott and A. R. Barron, *J. Am. Chem. Soc.*, 1993, **115**, 4971–4984.
27 D. E. Babushkin, N. V. Semikolenova, V. N. Panchenko, A. P. Sobolev, V. A. Zakharov and E. P. Talsi, *Macromol. Chem. Phys.*, 1997, **198**, 3845–3854.
28 P. L. Bryant, C. R. Harwell, A. A. Mrse, E. F. Emery, Z. Gan, T. Caldwell, A. P. Reyes, P. Kuhns, D. W. Hoyt, L. S. Simeral, R. W. Hall and L. G. Butler, *J. Am. Chem. Soc.*, 2001, **123**, 12009–12017.
29 Z. Falls, E. Zurek and J. Autschbach, *Phys. Chem. Chem. Phys.*, 2016, **18**, 24106–24118.
30 K. Von Lacroix, B. Heitmann and H. Sinn, *Macromol. Symp.*, 1995, **97**, 137–142.
31 J. L. Eilertsen, R. W. Hall, L. S. Simeral and L. G. Butler, *Anal. Bioanal. Chem.*, 2004, **378**, 1574–1578.
32 L. Rocchigiani, V. Busico, A. Pastore and A. Macchioni, *Dalton Trans.*, 2013, **42**, 9104–9111.
33 E. P. Talsi, N. V. Semikolenova, V. N. Panchenko, A. P. Sobolev, D. E. Babushkin, A. A. Shubin and V. A. Zakharov, *J. Mol. Catal. A Chem.*, 1999, **139**, 131–137.
34 Q. Wang, Y. Zhao, L. Song, Z. Fan and L. Feng, *Macromol. Chem. Phys.*, 2001, **202**, 448–452.
35 M. Bolesłławski, S. Pasynkiewicz, A. Kunicki and J. Serwatowski, *J. Organomet. Chem.*, 1976, **116**, 285–289.
36 J.-N. Pédeutour, K. Radhakrishnan, H. Cramail and A. Deffieux, *Macromol. Rapid Commun.*, 2001, **22**, 1095–1123.
37 C. J. Harlan, S. G. Bott and A. R. Barron, *J. Am. Chem. Soc.*, 1995, **117**, 6465–6474.
38 R. Glaser and X. Sun, *J. Am. Chem. Soc.*, 2011, **133**, 13323–13336.
39 M. Linnolahti, J. R. Severn and T. A. Pakkanen, *Angewandte Chemie International Edition*, 2008, **47**, 9279–9283.
40 F. Ghiotto, C. Pateraki, J. Tanskanen, J. R. Severn, N. Luehmann, A. Kusmin, J. Stellbrink, M. Linnolahti and

M. Bochmann, *Organometallics*, 2013, **32**, 3354–3362.
41 F. Ghiotto, C. Pateraki, J. R. Severn, N. Friederichs and M. Bochmann, *Dalton Trans.*, 2013, **42**, 9040–9048.
42 S. Collins and M. Linnolahti, *ChemPhysChem*, 2023, **24**, e202200759.
43 P. M. Castro, P. Lahtinen, K. Axenov, J. Viidanoja, T. Kotiaho, M. Leskelä and T. Repo, *Organometallics*, 2005, **24**, 3664–3670.
44 M. A. Henderson, T. K. Trefz, S. Collins, M. Y. Wang and J. S. McIndoe, *Organometallics*, 2013, **32**, 2079–2083.
45 T. K. Trefz, M. A. Henderson, M. Y. Wang, S. Collins and J. S. McIndoe, *Organometallics*, 2013, **32**, 3149–3152.
46 H. S. Zijlstra, M. Linnolahti, S. Collins and J. S. McIndoe, *Organometallics*, 2017, **36**, 1803–1809.
47 H. S. Zijlstra, S. Collins and J. S. McIndoe, *Chem. Eur. J.*, 2018, **24**, 5506–5512.
48 A. Joshi, H. S. Zijlstra, E. Liles, C. Concepcion, M. Linnolahti and J. S. McIndoe, *Chem. Sci.*, , DOI:10.1039/D0SC05075J.
49 S. Kaita, Z. Hou and Y. Wakatsuki, *Macromolecules*, 1999, **32**, 9078–9079.
50 C. M. Killian, D. J. Tempel, L. K. Johnson and M. Brookhart, *J. Am. Chem. Soc.*, 1996, **118**, 11664–11665.
51 S. A. Svejda and M. Brookhart, *Organometallics*, 1999, **18**, 65–74.
52 A. F. R. Kilpatrick, J.-C. Buffet, P. Nørby, N. H. Rees, N. P. Funnell, S. Sripothongnak and D. O'Hare, *Chem. Mater.*, 2016, **28**, 7444–7450.
53 L. V. Parfenova, P. V. Kovyazin and A. Kh. Bikmeeva, *Molecules*, , DOI:10.3390/molecules25092216.
54 H. S. Zijlstra, A. Joshi, M. Linnolahti, S. Collins and J. S. McIndoe, *Dalton Trans.*, 2018, **47**, 17291–17298.
55 A. Joshi, S. Collins, M. Linnolahti, H. S. Zijlstra, E. Liles and J. S. McIndoe, *Chem. Eur. J.*, 2021, **27**, 8753–8763.
56 A. Naim, M. Farenc, M. Hubert-Roux, T. Chavagnan, V. Cirriez, A. Welle, A. Vantomme, E. Kirillov, J.-F. Carpentier, C. Afonso and P. Giusti, *Anal. Chem.*, 2020, **92**, 2922–2925.
57 K. Giles, S. D. Pringle, K. R. Worthington, D. Little, J. L. Wildgoose and R. H. Bateman, *Rapid Commun. Mass Spectrom.*, 2004, **18**, 2401–2414.
58 K. Giles, J. P. Williams and I. Campuzano, *Rapid Commun. Mass Spectrom.*, 2011, **25**, 1559–1566.
59 J. Hofmann, W. B. Struwe, C. A. Scarff, J. H. Scrivens, D. J. Harvey and K. Pagel, *Anal. Chem.*, 2014, **86**, 10789–10795.
60 D. P. Smith, T. W. Knapman, I. Campuzano, R. W. Malham, J. T. Berryman, S. E. Radford and A. E. Ashcroft, *Eur. J. Mass Spectrom.*, 2009, **15**, 113–130.
61 C. Petucci and J. Diffendal, *J. Mass Spectrom.*, 2008, **43**, 1565–1568.
62 A. B. Kanu, P. Dwivedi, M. Tam, L. Matz and H. H. Hill Jr., *J. Mass Spectrom.*, 2008, **43**, 1–22.
63 F. Lanucara, S. W. Holman, C. J. Gray and C. E. Eyers, *Nature Chem.*, 2014, **6**, 281–294.
64 S. Hupin, H. Lavanant, S. Renaudineau, A. Proust, G. Izzet, M. Groessl and C. Afonso, *Rapid Commun. Mass Spectrom.*, 2018, **32**, 1703–1710.
65 A. S. Woods, M. Ugarov, T. Egan, J. Koomen, K. J. Gillig, K. Fuhrer, M. Gonin and J. A. Schultz, *Anal. Chem.*, 2004, **76**, 2187–2195.
66 C. Barrère, F. Maire, C. Afonso and P. Giusti, *Anal. Chem.*, 2012, **84**, 9349–9354.
67 C. Barrère, W. Selmi, M. Hubert-Roux, T. Coupin, B. Assumani, C. Afonso and P. Giusti, *Polym. Chem.*, 2014, **5**, 3576–3582.
68 M. Farenc, M. Witt, K. Craven, C. Barrère-Mangote, C. Afonso and P. Giusti, *J. Am. Soc. Mass Spectrom.*, 2017, **28**, 507–514.
69 Z. Wu, R. P. Rodgers and A. G. Marshall, *Anal. Chem.*, 2004, **76**, 2511–2516.
70 C. A. Hughey, C. L. Hendrickson, R. P. Rodgers, A. G. Marshall and K. Qian, *Anal. Chem.*, 2001, **73**, 4676–4681.
71 T. Fouquet and H. Sato, *Mass Spectrom (Tokyo)*, 2017, **6**, A0055.
72 O. Lacroix-Andrivet, S. Moualdi, M. Hubert-Roux, C. Loutelier Bourhis, A. L. Mendes Siqueira and C. Afonso, *J. Am. Soc. Mass Spectrom.*, 2022, **33**, 1194–1203.
73 A. G. Marshall and R. P. Rodgers, *Acc. Chem. Res.*, 2004, **37**, 53–59.
74 X. Ortiz, K. J. Jobst, E. J. Reiner, S. M. Backus, K. M. Peru, D. W. McMartin, G. O'Sullivan, V. Y. Taguchi and J. V. Headley, *Anal. Chem.*, 2014, **86**, 7666–7673.
75 M. Ubukata, K. J. Jobst, E. J. Reiner, S. E. Reichenbach, Q. Tao, J. Hang, Z. Wu, A. J. Dane and R. B. Cody, *J. Chromatogr. A*, 2015, **1395**, 152–159.
76 A. L. Myers, K. J. Jobst, S. A. Mabury and E. J. Reiner, *J. Mass Spectrom.*, 2014, **49**, 291–296.
77 K. J. Jobst, L. Shen, E. J. Reiner, V. Y. Taguchi, P. A. Helm, R. McCrindle and S. Backus, *Anal. Bioanal. Chem.*, 2013, **405**, 3289–3297.
78 D. Ohta, S. Kanaya and H. Suzuki, *Curr. Opin. Biotechnol.*, 2010, **21**, 35–44.
79 H. Sato, S. Nakamura, K. Teramoto and T. Sato, *J. Am. Soc. Mass Spectrom.*, 2014, **25**, 1346–1355.

80 A. C. Walker and E. J. Jr. Ernst, *Ind. Eng. Chem. Anal. Ed.*, 1930, **2**, 139–140.
81 A. Joshi, S. Donnecke, O. Granot, D. Shin, S. Collins, I. Paci and J. Scott McIndoe, *Dalton Trans.*, 2020, **49**, 7028–7036.
82 J. Stellbrink, A. Niu, J. Allgaier, D. Richter, B. W. Koenig, R. Hartmann, G. W. Coates and L. J. Fetters, *Macromolecules*, 2007, **40**, 4972–4981.
83 E. Endres, H. S. Zijlstra, S. Collins, J. S. McIndoe and M. Linnolahti, *Organometallics*, 2018, **37**, 3936–3942.